



OPEN

Snow cover detection using remote sensing techniques over different climate zones of Türkiye

Günay Çakır^{1,2}✉, Nuri Bozali^{1,3} & Fatih Sivrikaya^{1,4}

Snow-covered land surfaces can be easily mapped using remote sensing technologies. Accurate estimation of snow cover on the land surface allows for the construction of water resource management today. Using Landsat TM/ETM + satellite images, this study tried to assess how much snowfall covered the soil in Trabzon, Gümüşhane, and Bayburt provinces between 1999 and 2023. Satellite images were classified into three categories using the ERDAS 9.1 TM software. These classes are classified as snow-covered surfaces, other places, and data loss (cloud-shadow). When performing image analysis, it was important to verify that the cloudiness rate in the images was less than 15%. Images with cloudiness rates of more than 15% were not used. Seasonal and annual trend analysis of snow-covered areas (SCA) over three distinct regions (Trabzon, Gümüşhane, and Bayburt) were examined using the Mann-Kendall test. When three distinct study regions were examined together, Bayburt had the highest SCA rate, followed by Gümüşhane and Trabzon. In all three fields, the highest SCA was recorded in 2000, while the lowest SCA was recorded in 2017. The trends noticed that SCA on both annual and seasonal scales did not reach the statistical significance level of 0.05. Although snowfall in Trabzon, Gümüşhane, and Bayburt was beneficial in the autumn and spring seasons, no statistically significant association was found. The research concluded that the existing data are inadequate to make any statements on the impact of global warming in the area. However, the study figured out that satellite data may be effectively used to identify snowy places as a result of the study. Comparable investigations need to be undertaken in regions with varying climates, utilizing diverse remote sensing data and classification methodologies.

Keywords Climate, GIS, Landsat images, Remote sensing, Snowy area

Snowfall occurs when the air temperature is below 0 °C. Water vapor in the atmosphere condenses under high humidity conditions in a cold air mass and forms water droplets or ice crystals. These tiny water droplets and ice crystals merge and become larger grains. These enlarged particles, moving downwards under the influence of gravity, can reach temperatures below freezing as they pass through the air layers. When the temperature is appropriate, they descend to the earth and create precipitation¹.

Precipitation can vary in type, including rain, snow, hail, or sleet, based on the composition of the drops or crystals. This process takes place under varying climatic circumstances in the atmosphere. Precipitation, mostly in the form of snow at higher altitudes, is influenced by the temperature near the earth's surface. Snowfall is prevalent in regions with cold temperatures, high altitudes, and hilly terrain^{2–5}.

The high energy needed to melt snow can be supplied by the rise in air temperature during the snow melting period, although this process may be delayed. The static stability of the atmospheric layer over huge SCA prevents significant decreases in air temperature^{6,7}. SCA is essential to the earth's energy balance and hydrological cycle. Monitoring snowmelt and calculating snow water equivalent is crucial for precise water resource management. Snow models often need additional meteorological factors such as snow water equivalent, snow particle size, snow-covered regions, albedo, snow temperature profile, and solar radiation. Remote sensing images are often used to monitor changes in snow cover and detect snow-covered locations^{8–17}. Remote sensing methods have significant advantages in detecting SCA. Many researchers have determined snow-covered areas using remote sensing data¹⁸. Satellite images such as AVHRR, MODIS, MERIS, Landsat, and ASTER are the most widely used satellite images to determine snow-covered areas^{19,20}.

¹Department of Forestry, Gümüşhane Vocational School, Gümüşhane University, Gümüşhane, Turkey. ²Wildlife Ecology and Management Department, Faculty of Forestry, Karadeniz Technical University, Trabzon, Turkey. ³Forest Engineering Department, Faculty of Forestry, Karadeniz Technical University, Trabzon, Turkey. ⁴Forest Engineering Department, Faculty of Forestry, Kastamonu University, Kastamonu, Turkey. ✉email: gcakir@ktu.edu.tr

Satellite images containing thermal bands are used to distinguish SCA from other areas with the help of remote sensing techniques. Landsat 8 is a valuable satellite for processing images of SCA²¹. Research conducted in the Swiss Alps used Landsat TM satellite data to accurately determine the seasonal variation of the snow line in a short period²². The research in Japan used Landsat MSS satellite data and climatic trends to accurately predict that 90% of the melted snow water would flow into the river²³. The Landsat satellite images were used to monitor the change in snow cover area in 1975, 1988, and 2000. It was found that the snow cover area increased in 1975 (1,817,228.6 ha) and 2000 (1,874,945.7 ha) but decreased in 1988 (1,620,590.2 ha)²⁴. Research at Goose Lake in California used Landsat's 5-year (2017–2022) and 4-month (December–March) daily imagery to identify snow-covered regions. The results were matched with data from ground snow measuring sites, revealing an accuracy level of 76%²⁵.

In Türkiye, some studies have been carried out regarding snowy days and the periods in which snow falls, according to meteorological station data regarding snowfall. The spatial distributions of profitable days by KOÇ and KARTUM were monitored with 75-year meteorological station data²⁶. Akyürek and Şorman determined snow-covered areas in the Upper Euphrates River basin of Türkiye and in the altitude range of 1125–3500 m with NOAA AVHRR images²⁷. In these studies, 1-year application images or meteorological station data were used. Tekeli and his colleagues studied snowmelt in the Karasu basin of Türkiye's Eastern Anatolia Region in 2005 using MODIS satellite pictures. As a result, the researcher, whose primary goal is to predict snowmelt flow, needs the snow-covered area, which is a crucial input variable in big practical snowmelt flow models. MODIS or similar satellite images have shown to be an efficient option for Türkiye and most developing countries in this regard, functioning as a critical component in hydrological and meteorological forecast models²⁸.

The visible impacts of global warming include rising temperatures and less precipitation, causing geographical alterations in extensive snow cover. Tracking variations in snow cover aids in comprehending the potential for spring floods and summer droughts. One-third of the surface water from melted snow is utilized for agricultural irrigation. Its significance is growing steadily because of the impacts of snowmelt and associated surface runoff on floods, avalanches, landslides, and agricultural yields. Snowfall may cause agricultural goods and fertile fields in the region to freeze. Assessing the quantity of snowfall and SCA in a region might benefit farmers²⁵.

Advancements in technology have made it more convenient and cost-effective to employ remote sensing and satellite data to identify snow-covered areas, as opposed to traditional terrestrial methods. To study the impact of global warming on a specific location using satellite images, consistent monitoring of the region and access to precise, long-term meteorological data are essential. Few studies combine satellite images with climate data to determine SCA. This study used medium-resolution satellite images to identify SCA in regions across three distinct climate zones and examined their correlation with climate data. The main hypothesis of the study was that there was no change in snowfall for the three provinces. The study assessed the effect of climate change on snow cover by measuring the extent of SCA.

Materials and methods

Study area

The research region included three distinct provinces: Trabzon (4631.2 km²), Gümüşhane (6662.4 km²), and Bayburt (3741.4 km²) (Fig. 1). Trabzon is situated in the Eastern Black Sea Region, specifically between 40° 33' and 41° 07' north latitudes and 39° 07' and 40° 30' east longitudes. The elevation above sea level gradually rises towards the south and reaches a height of 3000 meters²⁹. Gümüşhane is situated in the Eastern Black Sea Region, with coordinates ranging from 38° 45' to 40° 12' east longitude and 39° 45' to 40° 50' north latitude. The average height of Gümüşhane is 1210 meters^{30,31}. Bayburt is situated in the northeastern region of Türkiye, namely in the interior areas of the Eastern Black Sea Region. Its coordinates range between 40° 45' and 39° 37' east-west longitudes and 40° 37' and 39° 52' north-south latitudes. The elevation of Bayburt is 1550 m above sea level³². The coastal part of the research region has a warm and wet environment, whereas the interior parts have a prevailing continental climate. With increasing altitude in the area, there is a corresponding reduction in temperature and a higher occurrence of snowfall.

Gümüşhane province is a transition between Eastern Anatolia and the Black Sea region in terms of climate characteristics and every aspect. Gümüşhane province, which prevents the oppressive humid air of the Black Sea with its high Zigana walls and the kop barrier that prevents the severe cold of Eastern Anatolia from coming, has a pleasant climate that has rare regions in the world. Our province has a continental climate between 39 and 41 degrees East Longitude and 40–41 degrees North Latitude in the inner part of the Eastern Black Sea Region. Wind: The annual average wind speed in our province is 9.9 (m/sec). The annual dominant wind blows from the west. The average number of clear and sunny days in Gümüşhane is 79 days. The average number of closed days is 68 days. The most sunshine is in July, the least in January and December. Winter and spring are the rainy seasons in the province. However, precipitation is generally in the form of snow in winter and rain in spring³³.

In Trabzon, a temperate climate is observed in the coastal area due to the effect of the sea. Summers are moderate, and winters are pleasant. The Caucasus Mountains border Trabzon from the south, preventing cold northwest winds from entering Siberia and chilling the air in northeastern Anatolia. Trabzon province has two different climatic types. While a warm and rainy climate is prevalent along the coast, the continental climate dominates in the interior. The data from the Maçka meteorological station (altitude: 250 m) were utilized to demonstrate a continental climate. For the coastline area statistics, data from the meteorological station in Trabzon city centre (altitude: 30 m) were used³³.

In Bayburt, a transitional climate with continental characteristics prevails between the Eastern Black Sea climate and the Eastern Anatolian climate. For this reason, summers are hot and dry, and winters are cold and rainy. However, due to the low average altitude and the “Microclimate” formed by the valley system, the climate is milder than in Eastern Anatolia. Summer days generally occur between May and September. Rainy days in

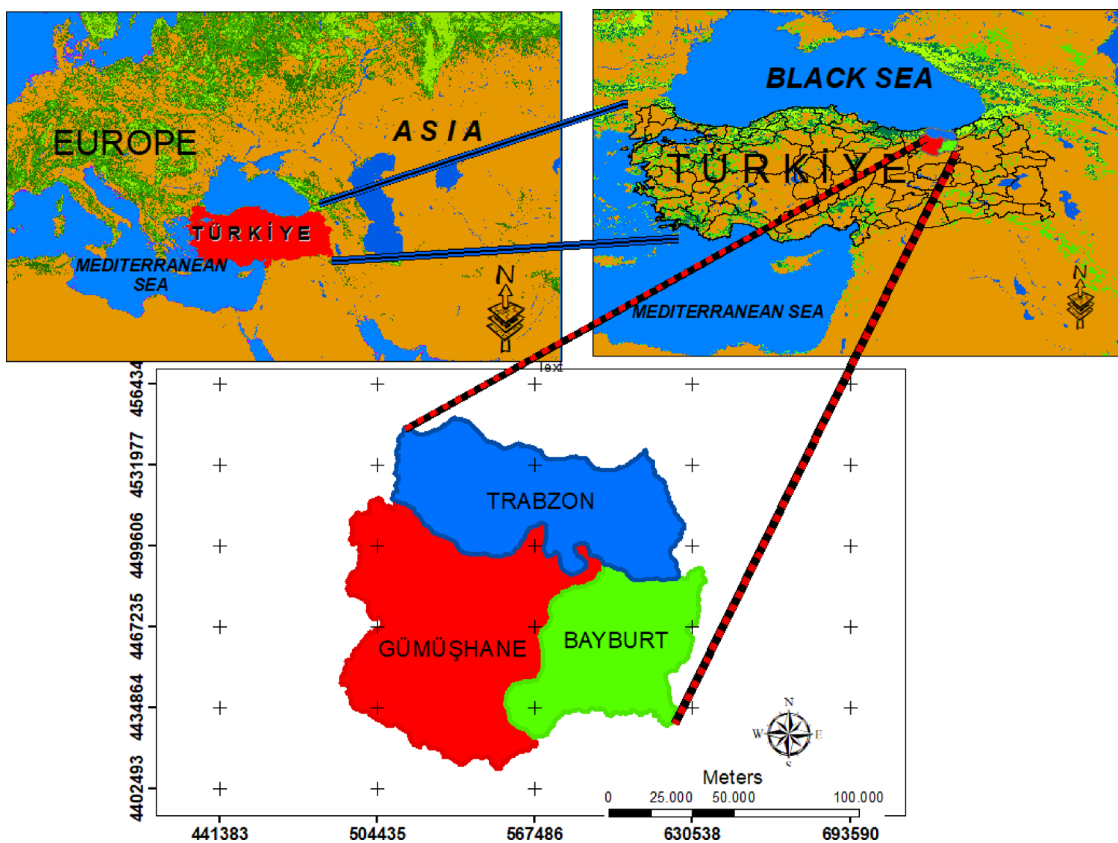


Fig. 1. Study area.

Bayburt are 102, and the average rainfall is 433.4 mm. The highest temperature is 36.2 C (20.07.1962), the lowest temperature is – 26.2 C (29.01.1964), and the average temperature is 7.0 degrees C³³.

Dataset and image processing

Landsat (TM, ETM+, and OLI) satellite images between 1999 and 2023 were obtained free of charge from the available for download in full tile bundles or individual files from EarthExplorer (<https://earthexplorer.usgs.gov>), an open-source satellite image provider that provides data internationally. The data are located under the Landsat category. Landsat Collection 2 is a Level-2 subcategory, and it is listed as Landsat 4–5 TM, Landsat 7 ETM+, and Landsat 8–9 OLI/TIRS (Table 1)³⁴. Since the photos obtained from this database had already undergone geometrical and radiometric correction, no augmentation was necessary. The reference confirmation for the study area was the geographic coordinate grid WGS84.

Distinguishing snow from clouds is the most crucial problem in detecting SCA using satellite images. In satellite images, images with cloudiness below 15% were preferred in this study. Therefore, images with a cloudiness level of over 15% were excluded from evaluation. In addition, since the acquisition dates of some satellite images were in the first or last days of the month, no images were taken in the following month. The SCA in months with two images was determined by calculating the average of the two values. The monthly average meteorological data was obtained from the General Directorate of Meteorology (MGM), which was used to compare the SCA with meteorological data (Table 2).

Snowy areas are separated better than other surfaces in these band values. Satellite images show SCA in Snow possesses various spectral properties from other land feature classes like clouds, etc. Snow typically has a high reflectance in the visible band (0.6–0.8 μ m), which gives it its distinct spectral properties³⁵. Since the reflectance of snow is very high in the visible part of the spectrum (corresponding to band two centered at wavelength 0.56 μ m), it is close to zero in the short-wave infrared part of the spectrum (corresponding to band 5 centered at wavelength 1.65 μ m). This study used band 2 and 5 data to detect SCA. SCA are difficult to distinguish from cloudy areas. Moreover, the most effective approach to overcome the cloud obstacle is to use a wavelength of 1.60 μ m in the near-infrared spectrum, together with a visible band gap^{36,37}.

228 satellite images taken between 1999 and 2023 were examined. The study area includes a single satellite image frame. Snow cover analyses were performed from new images cut from the outer border of this area. Single-band images of the study area and multi-band images were obtained with the layer stack using ERDAS Imagine 9.1 software. Following the Landsat data collection, Erdas Imagine 9.1 TM was used to analyze the images in order to extract changes in the snow cover, cloud (no data), and other areas. Although the option of having cloudiness rates below 15% was chosen in the satellite imagery used for snow cover areas, the classification

Years	Image gathering date*											
	Jan	Feb	Mar	Apr	May	Jun	Jul	Aug	Sep	Oct	Nov	Dec
1999	28	13	17	18			17		19	5	4	6
2000	7		19	20	22	15	17	28	15		22	
2001	9	10	6				12	5	22	8		19
2002	28	5	25	26	20		2	8	25	11	28	14
2003							2	27		14	15	
2004	18	27	22	7	25		12	5	14	8	1	27
2005	20	13		10	12		23	16	1			6
2006			28	15	31	16	26	27	20	6		9
2007		11		8	18	27	5	6	15	1	10	
2008	13		1		20	5	21		25		12	14
2009	23		4	5	15	8	10		12		23	1
2010			23	16	18		13	6	15		2	20
2011	13	22	26				24	1	18	4		
2012		25	28	29		16	18	3	20	6	7	9
2013	10		21	24	26			30	15	9	18	28
2014	5	6	18		2		24	17	25		13	
2015	24			6		17	27	20	13		16	18
2016	3	4	7	8	2	27	13	30	15	1	18	20
2017				27	29	30	16		18	20	13	
2018	8	1	13	6	16	9	3	20	5	7	8	
2019	19	4	8	9	27	12	14	15	16	10	11	
2020	14		2	14	21	22	16	25	18	23	29	7
2021		1	29	11	28	1	19	4	21	23	8	26
2022	3	12		25	11	20	30	31	16	2	7	29
2023	22		22	25	17	8	1	26	27	29		

Table 1. Satellite image acquisition dates between 1999–2023.

accuracy was improved because the study generally supplied images with cloudiness rates below 5%. Snow-covered satellite images were analyzed, but uncovered snow satellite images were left unprocessed (Fig. 2).

The Normalized Difference Snow Index (NDSI) is determined as the difference in reflectance measured in a visible band (often green) and a short-wave infrared (SWIR) band divided by the total reflectance of the two bands³⁸. NDSI is based on snow and ice's spectral properties, which include a high visible-light reflectance and a strong SWIR absorption. It has historically been used to calculate NDSI using the green wavelength range (0.52–0.60 mm) and SWIR (1.55–1.75 mm), which are popular in many current sensors. The equation is used to compute NDSI (NDSI= (Green-SWIR) / (Green+SWIR))³⁹. The values of the NDSI index range from 1 to -1 within the theoretically conceivable range of snow³⁸. The clouds may also have positive NDSI values, which typically range between -0.4 and 0.4⁴⁰. As a result, a lower NDSI score makes it more difficult to discern between clouds and snow.

These classes were determined using an unsupervised classification method. In the image generated using unsupervised classification, red represents snowy areas, and black shows and other areas. In the study area, snow-covered areas and other areas are divided into three classes. Acceptable classification accuracy values were over 90%. In addition, these images in which there is no snowfall in summer are not classified, and adding to the table no snowfall values. Since three class values were used for the snow-covered surface and other areas, produce accuracy and user accuracy were high. The workflow diagram for the study is given in Fig. 3.

The SCA for Trabzon, Gümüşhane, and Bayburt in different periods (autumn, winter, spring, summer, and annual average) was determined by analyzing monthly Landsat satellite images between 1999 and 2023. The Mann-Kendall trend test, a quantitative analytical technique, was employed to assess the importance of shifting trends in time series, while the Mann-Kendall mutation test was utilized to identify the locations of mutation points within the time series. The Mann-Kendall test facilitates the assessment of trend characteristics and ratios, rendering them utilized in hydro-climatic research. The Mann-Kendall test was employed to analyze variations in SCA trends across several temporal intervals (fall, winter, spring, summer, and yearly average) in this study.

Results

SCA for Trabzon, Gümüşhane, and Bayburt were determined by analyzing monthly Landsat satellite images between 1999 and 2023. Table 3 shows the average SCA ratio for Trabzon, Gümüşhane, and Bayburt by seasons (autumn, winter, spring, and summer) and annual average. The annual average SCA was calculated for the regions as presented in Fig. 4. The SCA ratio shows significant changes from year to year as a result of fluctuations in both precipitation and temperature. The 25-year average SCA ratio in Trabzon is 19.2%, 5.4% in autumn,

			Climate Data Periods (1927–2022)											
			Jan	Feb	Mar	Apr	May	Jun	Jul	Aug	Sep	Oct	Nov	Dec
Average temp (°C)	TRB	7.5	7.3	8.4	11.8	15.9	20.2	23.0	23.4	20.5	16.7	13.0	9.6	14.8
	GUM	-1.8	-0.5	3.6	9.3	13.6	17.1	20.0	20.2	16.4	11.2	5.0	0.5	9.6
	BAY	-6.2	-4.9	0.4	7.0	11.6	15.3	18.8	18.8	14.8	9.3	2.8	-3.0	7.1
Average max. temp (°C)	TRB	10.8	10.8	11.9	15.6	19.2	23.2	26.0	26.6	23.8	20.1	16.5	13.0	18.1
	GUM	3.0	5.3	9.9	16.3	21.2	25.2	28.2	29.0	25.4	18.9	10.7	4.9	16.5
	BAY	-0.9	0.7	5.9	13.2	18.4	22.9	27.2	27.8	23.6	16.9	8.8	1.9	13.9
Average min. temp (°C)	TRB	4.7	4.4	5.4	8.7	12.9	17.1	20.0	20.4	17.4	13.7	10.1	6.8	11.8
	GUM	-5.5	-4.8	-1.1	3.8	7.6	10.9	13.9	13.9	10.2	6.0	0.9	-3.0	4.4
	BAY	-10.5	-9.2	-4.1	1.8	5.7	8.4	11.2	11.1	7.4	3.6	-1.8	-6.9	1.4
Average sunny day (hours)	TRB	2.7	3.3	3.4	4.4	5.6	7.1	5.9	5.6	4.9	4.5	3.6	2.7	4.5
	GUM	1.4	3.8	4.9	6.0	7.3	8.9	9.9	9.5	7.9	5.4	2.3	1.2	5.7
	BAY	-	-	-	-	-	-	-	-	-	-	-	-	-
Average rainy days	TRB	12.20	11.95	13.20	12.84	12.64	10.69	7.89	8.67	10.77	12.25	11.78	12.34	137.2
	GUM	11.31	10.51	12.82	13.56	15.41	10.62	4.08	3.80	5.49	9.44	9.93	11.46	118.4
	BAY	11.20	10.91	12.86	13.84	15.77	10.63	5.05	4.44	5.02	8.72	8.86	10.98	118.3
Sum of monthly rainy values (mm)	TRB	83.1	63.9	59.7	56.5	52.2	51.8	35.5	48.2	78.9	113.6	99.6	85.0	828.0
	GUM	36.4	31.0	44.4	57.7	68.2	48.0	12.7	14.2	21.6	43.2	42.0	40.9	460.3
	BAY	27.1	27.7	42.0	62.0	72.2	51.4	21.2	16.2	22.1	43.2	32.7	29.2	447.0
Max. Temp (°C)	TRB	27.0	30.1	35.2	37.6	38.2	36.7	37.0	38.2	37.9	33.8	32.8	26.4	38.2
	GUM	15.5	18.0	24.0	29.0	34.4	36.2	41.0	41.1	37.7	32.0	22.2	19.2	41.1
	BAY	11.0	13.9	21.2	25.3	31.3	34.7	37.0	38.4	34.4	28.8	20.0	18.2	38.4
Min. Temp (°C)	TRB	-7.0	-7.4	-5.8	-2.0	4.2	9.2	11.0	13.5	7.3	3.4	-1.6	-3.3	-7.4
	GUM	-23.6	-25.7	-22.6	-11.0	-2.8	1.8	4.5	4.9	-1.0	-4.8	-15.0	-21.0	-25.7
	BAY	-31.3	-27.6	-28.3	-12.7	-4.4	-1.6	0.2	2.4	-2.1	-10.6	-23.6	-29.0	-31.3

Table 2. Some meteorological variables for the research area. TRB, Trabzon; GUM, Gümüşhane; BAY, Bayburt.

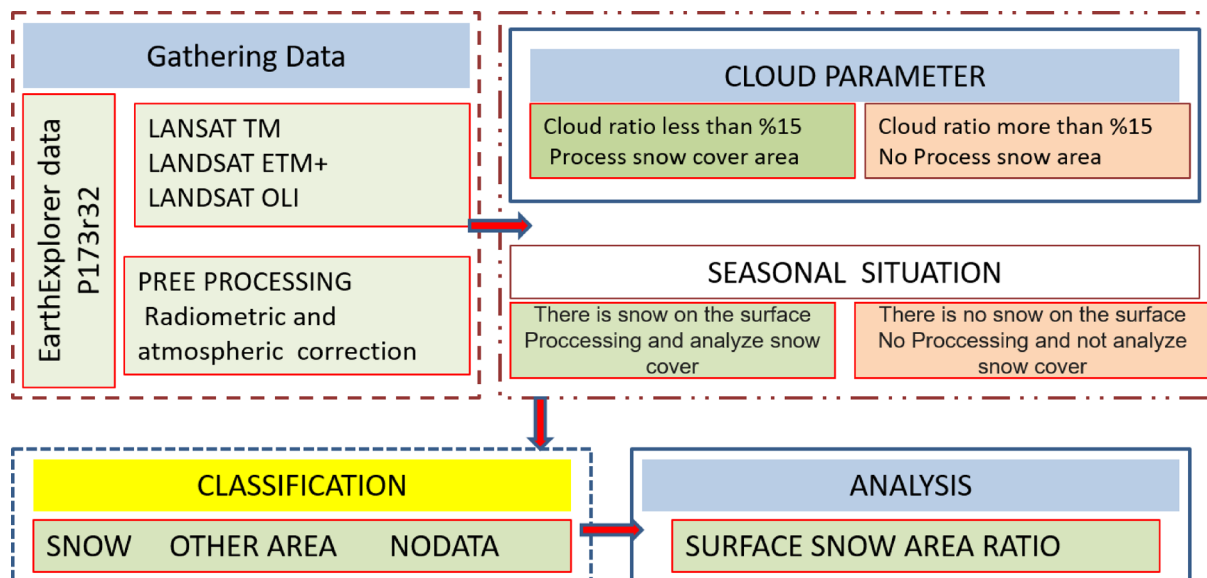


Fig. 2. The flowchart of the study.

58.2% in winter, 23.3% in spring, and 0.2% in summer. When the annual SCA is examined by years, the highest amount occurred in 2016 at 28.3%, and the lowest was 5.6% in 2017.

In winter, the highest amount was in 2000 at 85.0%, and the lowest was 30.5% in 2006. In Gümüşhane, the 25-year average SCA rate is 24.2%, 5.6% in autumn, 76.3% in winter, 27.8% in spring, and 0.2% in summer. When the annual SCA is examined by years, the highest amount occurred at 37.8% in 2005 and the lowest at 7.1% in 2017. The highest amount for winter was 100.0% in 2000 and 2002, and the lowest was 27.5% in 2006. In Bayburt,

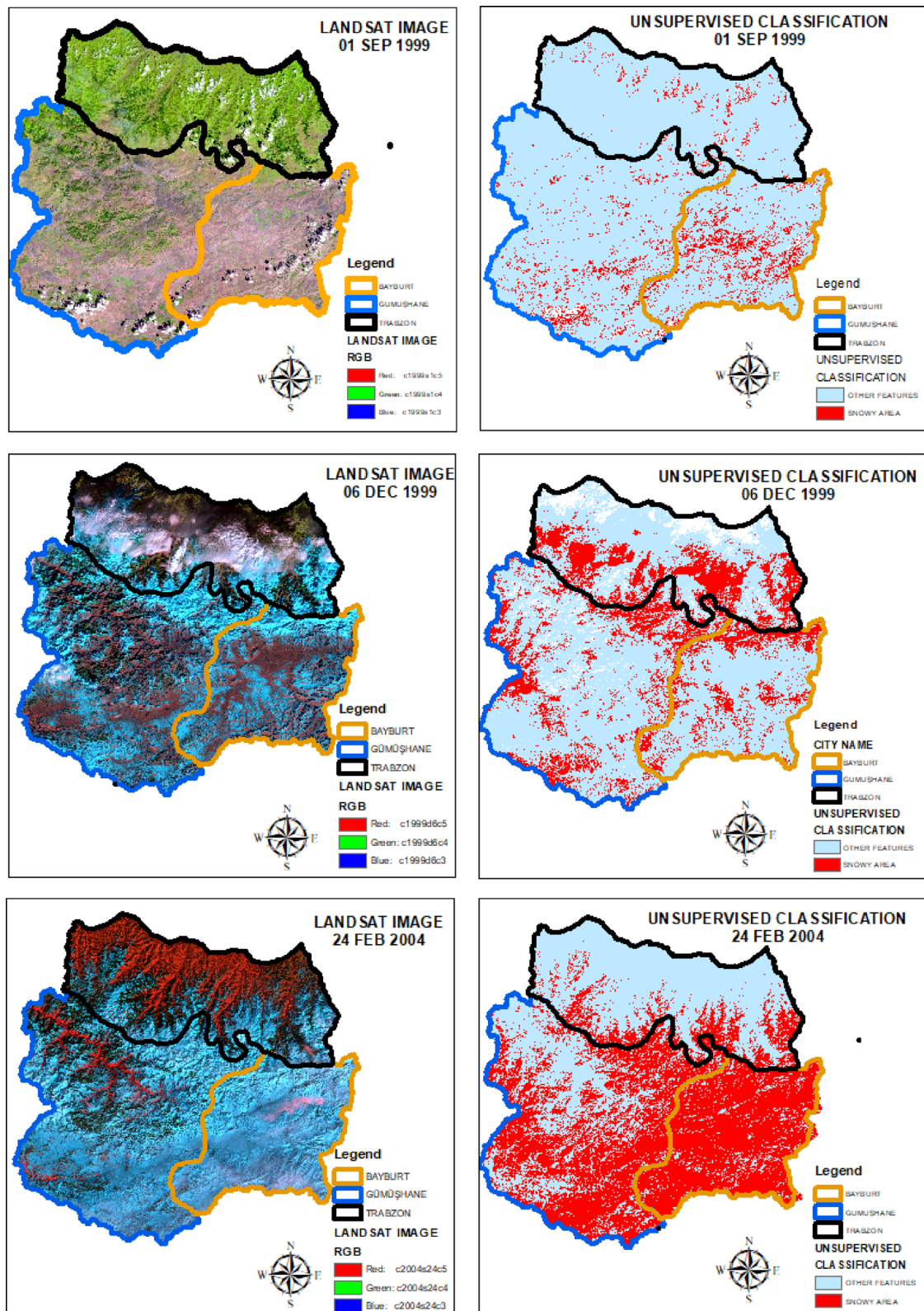


Fig. 3. Landsat satellite images and unsupervised classification of the study area.

Year	Trabzon					Gümüşhane					Bayburt				
	Average	Autumn	Winter	Spring	Summer	Average	Autumn	Winter	Spring	Summer	Average	Autumn	Winter	Spring	Summer
1999	24.2	1.3	46.7	49.0	0.0	29.6	1.0	65.0	49.0	0.0	29.5	0.7	64.3	50.0	0.0
2000	16.8	0.7	85.0	27.0	0.0	21.3	2.0	100.0	35.3	0.3	21.3	2.0	100.0	35.3	0.3
2001	11.0	1.7	35.0	7.3	0.0	16.0	0.7	56.3	6.7	0.3	16.3	0.3	58.0	6.3	0.3
2002	27.8	6.7	72.7	20.0	0.0	35.5	6.7	100.0	17.5	0.0	30.0	21.7	66.7	17.5	0.0
2003	12.5	10.0		45.0	0.0	21.7	20.0		70.0	0.0	27.5	25.0		90.0	0.0
2004	22.8	0.0	73.3	17.3	0.7	31.2	0.0	95.0	29.0	0.7	32.0	0.0	98.3	29.0	0.7
2005	27.3	0.0	62.0	16.0	0.0	37.8	0.0	82.7	26.5	0.5	37.5	0.0	82.0	26.5	0.5
2006	11.9	0.5	30.5	22.0	0.3	12.4	0.5	27.5	27.5	0.3	12.1	0.5	26.5	27.0	0.3
2007	20.3	8.3	70.0	36.0	0.0	25.6	11.7	94.0	42.3	0.0	27.2	15.0	95.0	44.0	0.0
2008	25.6	0.7	77.5	36.0	0.5	32.1	0.7	97.5	45.5	0.5	33.0	0.7	97.5	49.5	0.5
2009	21.6	16.7	47.5	31.0	0.0	29.0	23.3	72.5	34.7	0.0	29.1	20.0	72.5	38.3	0.0
2010	15.9	4.5	46.0	6.0	0.0	18.6	3.0	56.0	6.0	0.0	18.5	2.0	56.7	5.5	0.0
2011	19.5	14.0	42.3	22.5	0.0	21.4	10.0	50.0	27.5	0.0	21.5	10.3	51.0	26.0	0.0
2012	23.2	0.0	69.0	46.5	0.3	28.7	0.0	92.5	50.5	0.3	28.4	0.0	92.5	49.0	0.3
2013	20.4	2.3	82.0	17.3	0.3	20.1	1.3	90.0	12.3	0.0	21.4	1.0	95.0	14.0	0.0
2014	21.4	23.3	54.0	18.7	0.3	21.5	8.7	71.5	22.0	0.3	23.3	7.3	84.0	21.7	0.3
2015	22.9	4.5	71.5	30.0	0.3	26.5	3.0	85.0	35.0	0.3	27.5	3.0	94.0	25.0	0.3
2016	28.3	17.0	76.0	19.7	0.3	36.1	23.0	96.7	24.3	0.3	36.8	26.3	96.7	24.0	0.3
2017	5.6	0.7	40.0	3.5	0.3	7.1	0.3	50.0	6.0	0.3	7.9	0.7	65.0	2.0	0.0
2018	14.0	1.0	59.0	10.7	0.3	15.0	0.7	71.5	6.3	0.3	16.4	0.7	79.0	6.3	0.3
2019	22.3	4.3	64.0	34.3	0.3	28.5	5.0	92.5	37.7	0.3	31.1	6.7	97.0	42.3	0.3
2020	14.4	2.0	39.0	19.7	0.5	19.4	2.0	57.5	24.0	0.5	20.8	2.3	55.0	30.0	0.5
2021	15.0	0.7	43.5	25.3	0.0	20.7	0.3	71.5	28.0	0.0	22.6	1.0	77.5	30.3	0.0
2022	19.7	7.0	59.3	9.0	0.0	26.6	5.0	85.0	11.5	0.0	29.7	7.3	94.3	11.0	0.0
2023	14.7	7.7	50.0	13.0	0.0	21.5	11.0	71.5	19.7	0.3	23.7	14.7	74.0	22.7	0.3
Overall	19.2	5.4	58.2	23.3	0.2	24.2	5.6	76.3	27.8	0.2	25.0	6.8	78.0	28.9	0.2

Table 3. Seasonal and annual average of SCA for Trabzon, Gümüşhane and Bayburt.

the 25-year average SCA rate is 25.0%, 6.8% in autumn, 78.0% in winter, 28.9% in spring, and 0.2% in summer. When the annual SCA is examined by years, the highest amount occurred at 37.5% in 2005 and the lowest at 7.9% in 2017. In winter, the highest amount was 100.0% in 2000, and the lowest was 26.5% in 2006.

Upon evaluating three distinct study regions together, it was determined that Bayburt exhibited the greatest SCA rate, followed by Gümüşhane and Trabzon. This outcome is associated with the climate (temperature and precipitation) in the research regions. It was established that 2000 had the highest SCA across all three areas, while 2017 recorded the lowest SCA.

Bayburt province has a higher average elevation above sea level than the other two research areas. Trabzon Province has a coastline due to air mass movements. As a result, even in the winter, the temperature of seawater does not dip below +5 degrees Celsius. As a result, it reduces snowfall by up to 750 m. Gümüşhane province offers a medium altitude, comparable to both provinces. For these reasons, it ranks between the two provinces in terms of snowfall rate.

This work employed Mann-Kendall and Sen's slope methodology to assess the annual variation of SCA from 1999 to 2023, taking into account both annual and seasonal time scales (Table 4; Fig. 5). The patterns found for SCA at both annual and seasonal scales did not achieve a statistical significance level of 0.05. In Trabzon, SCA showed an increasing trend in autumn and summer and a decreasing trend in winter and spring. Kendall tau values for Trabzon are 0.156, -0.123, -0.211, and 0.216 for autumn, winter, spring, and summer, respectively. Sen's slope values are 0.073%/year, -0.380%/year, -0.540%/year, and 0.000%/year. In Gümüşhane, SCA showed an increasing trend in autumn and summer and a decreasing trend in winter and spring. Kendall tau values for Gümüşhane are 0.088, -0.155, -0.234, and 0.053 for autumn, winter, spring, and summer, respectively. Sen's slope values are 0.048%/year, -0.395%/year, -0.688%/year and 0.000%/year. In Bayburt, SCA showed an increasing trend in autumn, winter, and summer and a decreasing trend in spring. For Bayburt, Kendall tau values for autumn, winter, spring, and summer are 0.150, 0.004, -0.224, and 0.012, respectively. Sen's slope values are 0.053%/year, 0.019%/year, -0.659%/year and 0.000%/year. In Trabzon, Gümüşhane, and Bayburt, autumn and spring showed a positive trend, but no statistically significant relationship was found. The study investigated fluctuations in snowfall based on geographical location and discovered that they were directly tied to general air masses. Between November and April, air masses from Siberia had been observed to cause snowfall. Although snowfall decreased between 2011 and 2016, there was no substantial change in the amount of snow falling in the region in subsequent years.

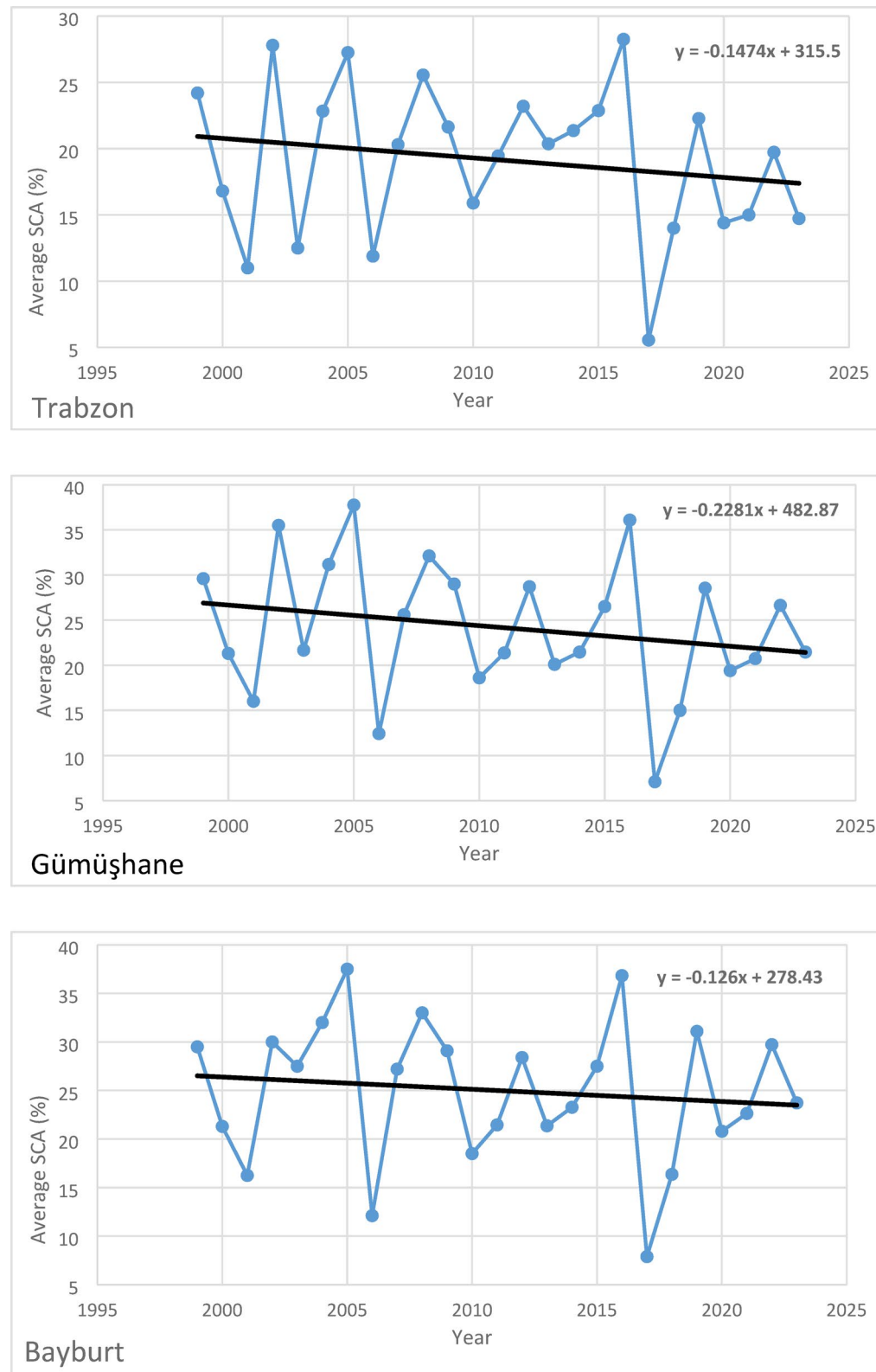


Fig. 4. Annual average SCA variability for Trabzon, Gümüşhane, and Bayburt.

Discussion

Research has shown a clear connection between the fluctuation of snow-covered regions and climate factors, particularly temperature. It has been highlighted that snow cover is very responsive to changes in temperature variables⁴¹. A robust inverse relationship was discovered between temperature and the extent of snow-covered

City	Period	Kendall's tau	Sen's slope
Trabzon	Average	-0.120	-0.148
	Autumn	0.156	0.073
	Winter	-0.123	-0.380
	Spring	-0.211	-0.540
	Summer	0.216	0.000
Gümüşhane	Average	-0.144	-0.166
	Autumn	0.088	0.048
	Winter	-0.155	-0.395
	Spring	-0.234	-0.688
	Summer	0.053	0.000
Bayburt	Average	-0.063	-0.083
	Autumn	0.150	0.053
	Winter	0.004	0.019
	Spring	-0.224	-0.659
	Summer	0.012	0.000

Table 4. Mann-Kendall test results for Trabzon, Gümüşhane and Bayburt.

surface in the Ganges River basin. According to⁴² it has been hypothesized that rising temperatures are a contributing factor to the reduction of snow-covered areas. Multiple studies indicate a favorable correlation between land elevation and the extent of snow-covered area, snow depth, and snow water equivalent. The references cited are Gurung et al.⁴³, Liu and Chen⁴⁴, Lopez-Moreno and Stahli⁴⁵, Rohrer et al.⁴⁶, and Woo and Thorne⁴⁷. Huang et al.⁴⁸ conducted a study examining the impact of variations in snow cover on the Tibetan Plateau from 2001 to 2014 on climate. The findings revealed an increase in snow-covered areas at elevations below 2000 m, whereas a decrease was observed above 2000 m. Through the observation of snow cover variations in the upper Indus Basin between 1984 and 2020, researchers discovered that the long-term impact of global warming became evident, resulting in adverse consequences for the region's snow and glaciers. Over 36 years, researchers noticed a correlation between the progression of global warming and the absence of snowfall in certain areas in 2020, as opposed to 1984⁴⁹.

The NDSI analysis methods performed best in snow cover areas with low bias and the best results over the investigated snow cover and canopy cover ranges⁵⁰. The process of mapping snow cover using data gathered by multi-spectral satellites has advanced with the development of a number of methodologies. Understanding how different approaches perform over different snow cover fractions and landscapes is crucial for recognizing global snow mapping capabilities, as snow cover varies at finer spatial resolution than multi-spectral sensors can record⁵⁰. Upon analysis of the data, it was seen that there was no anticipated reduction in the extent of snow cover in high-altitude regions within the research area. Nevertheless, it would be inaccurate to claim that global warming does not impact this area, given this discovery. According to several experts, while there may be occasional decreases in temperature, the general climate pattern indicates a tendency for temperatures to increase^{51,52}.

Both random forest-based conventional machine learning and U-Net-based deep learning for the semantic segmentation challenge using Sentinel-2 images were used for snow coverage mapping. A U-Net-based deep learning classifier utilizing four informative spectral bands is deemed appropriate for snow coverage mapping⁵³. In a comparable manner, snow cover was effectively assessed utilizing U-Net based models with the CSWV_S6 and Landsat 8 OLI datasets⁵⁴. Nonparametric artificial neural networks (ANN) and support vector machine (SVM) approaches for forest stand classification (FSC) mapping utilizing MODIS and Landsat 7 ETM + imagery were assessed for fractional snow cover. Surface reflectance values of MODIS bands 1–7, NDSI, and NDVI serve as predictor variables. Conversely, the reference FSC values are derived from Landsat ETM + data with superior resolution and serve as response variables. The independent test area indicates that the MLP-tansig model performs optimally. The SVM-RBF model performs inferiorly compared to the MLP-tansig model⁵⁵.

Conclusion

When examining the impact of global warming on a specific location using satellite images, it is necessary to regularly examine the area and have access to long-term, continuous, and highly accurate meteorological data for that region. The research concluded that the existing data are inadequate to make any statements on the impact of global warming in the area. However, the study found that satellite data may be effectively used to identify snowy places as a result of the study. Even though an analysis of snow's available impact was carried out, climate zones are mainly introduced for well-developed areas. However, snow formation occurs throughout the world, and its characteristics may significantly vary depending on climate conditions.

In this study, we used Landsat images to examine if snowfall in three provinces has changed by month between 1999 and 2023. Significant values were discovered when statistical analysis was conducted based on the area's percentage of snow cover at different land cover densities. This measure has demonstrated accuracy in classifying snow cover by season. Over a 25-year period, no discernible change in snowfall was discovered in the studied area using satellite image analysis. We are unable to discuss how climate change has affected the water

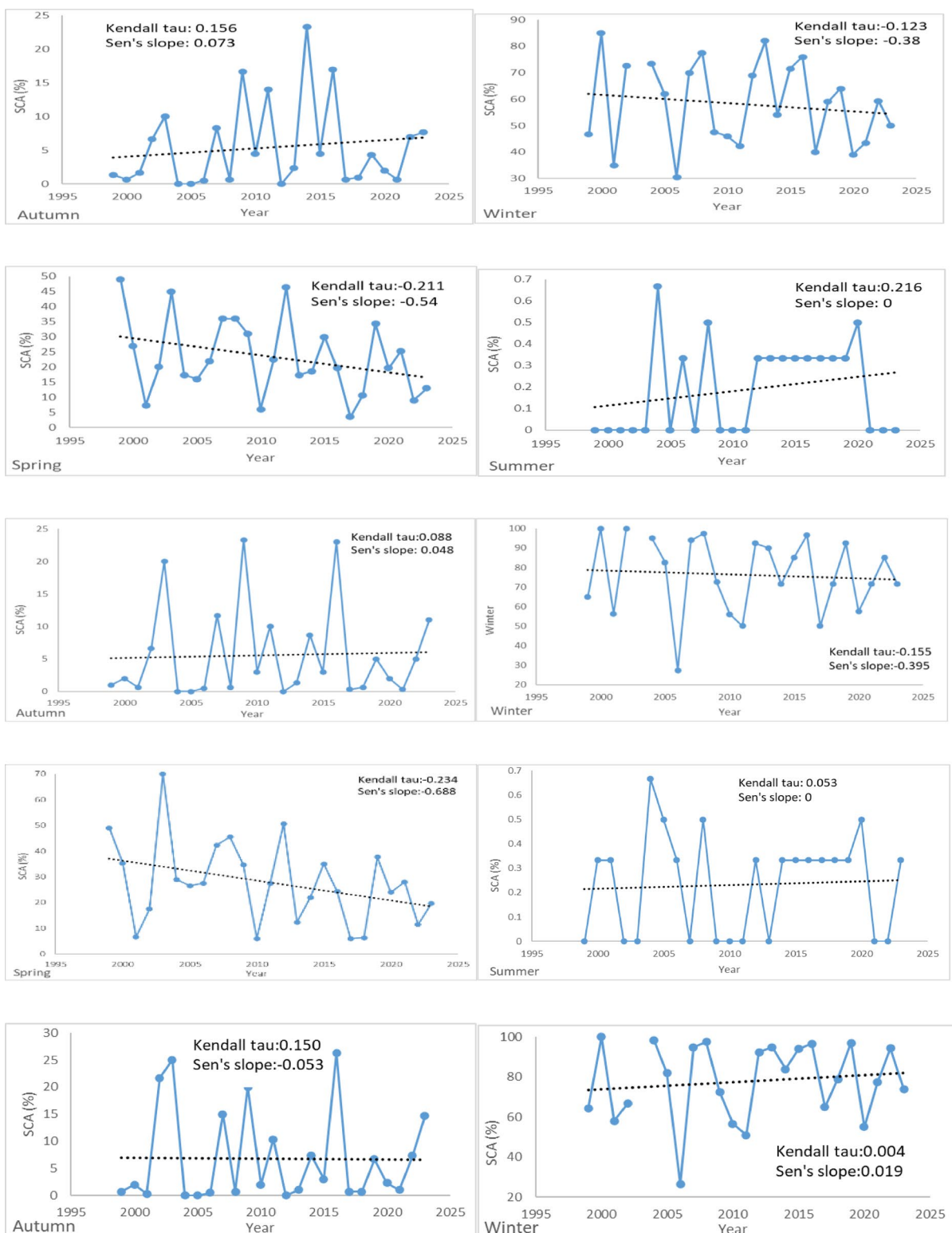


Fig. 5. Mann-Kendall trend of annual SCA derived from Landsat data in Trabzon, Gümüşhane, and Bayburt over a 25-year period (1999–2023).

cycle in any meaningful way in any of the three provinces that make up the Eastern Black Sea region. However, in the upcoming years, it will be important to keep up with the developments. The region's dense green tissue, which has slowed the rate of change, is its most noteworthy feature since forests are among the water cycle's most crucial components. Even though the three provinces have diverse climates, the continental and Black Sea climates dominate the study region. Depending on the altitude of snow-covered terrain, it covers a broader range

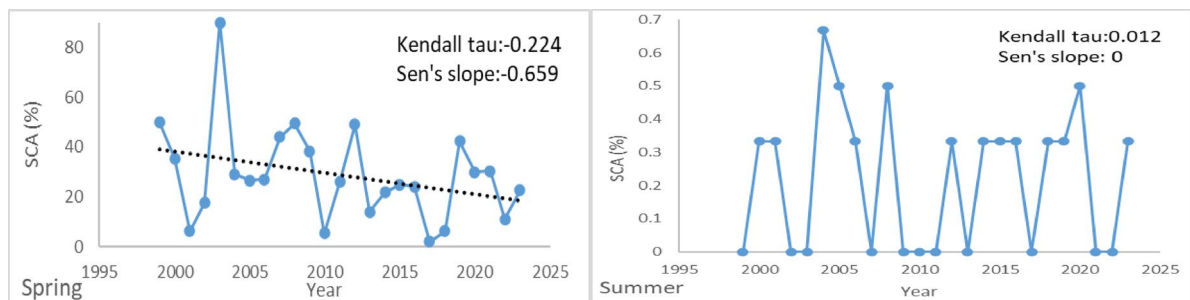


Fig. 5. (continued)

in the provinces of Bayburt and Gümüşhane. Snowfall has been heavy in coastal areas in recent years due to Siberian low pressure. The mountains in the Eastern Black Sea region run parallel to the sea, causing structural changes in air currents.

This study has some limitations. First of all, it is challenging to generalize for areas with varying climatic conditions because the investigation was restricted to just three provinces (Trabzon, Gümüşhane, and Bayburt). Furthermore, the removal of images with cloud cover percentages higher than 15% would have compromised the integrity of the time series analysis and resulted in data problems, particularly during the winter and spring seasons. The classification technique, which relies on conventional thresholds, has demonstrated poor performance when it comes to cloud-shadow discrimination or the detection of snow-covered regions with intricate land cover. The accuracy and usefulness of snow cover mapping should be enhanced for future research by utilizing satellite systems that provide regular data (such as MODIS and Sentinel), and the classification stage should incorporate machine learning (ML) and deep learning (DL) techniques. More thorough research employing multi-source data in various climatic zones in Türkiye will yield more comprehensive knowledge, even though the current work only offers a basic analysis.

Data availability

Data availability All data generated or analyzed during this study are included in this published article.

Received: 22 January 2025; Accepted: 12 June 2025

Published online: 04 July 2025

References

1. Simpson, G. C. The water in the atmosphere. *Sci. Monthly.* **20**(6), 621–629 (1925).
2. Kaser, G. Modern glacier retreat on Kilimanjaro as evidence of climate change: Observations and facts. *Int. J. Climatol. J. R. Meteorol. Soc.* **24**(3), 329–339. <https://doi.org/10.1002/joc.1008> (2004).
3. Hemp, A. Climate change-driven forest fires marginalize the impact of ice cap wasting on Kilimanjaro. *Glob. Change Biol.* **11**(7), 1013–1023. <https://doi.org/10.1111/j.1365-2486.2005.00968.x> (2005).
4. Molg, T., Cullen, N. J., Hardy, D. R., Winkler, M. & Kaser, G. Quantifying climate change in the tropical midtroposphere over East Africa from glacier shrinkage on Kilimanjaro. *JCLI* **22**(15), 4162–4181. <https://doi.org/10.1175/2009JCLI2954.1> (2009).
5. Brown, R. D. & Mote, P. W. The response of Northern hemisphere snow covers to a changing climate. *J. Clim.* **22**(8), 2124–2145. <https://doi.org/10.1175/2008JCLI2665.1> (2009).
6. Cohen, J. & Rind, D. The effect of snow covers on the climate. *J. Clim.* **4**(7), 689–706 (1991).
7. Cohen, J. Snow cover and climate. *Weather* **49**(5), 150–156. <https://doi.org/10.1002/j.1477-8696.1994.tb05997.x> (1994).
8. Ostrem, G. Snow and ice proceedings of a post graduate summer school on remote sensing. University of Dundee. ESA. SP-216 (1984).
9. Dinç, U., Dinç, O., Peştemalci, V., Yeğenigil, İ. & Şenol, S. Toros Dağlarında Bir Örnek Bölgede Kar Örtüsünün Landsat-5 Tm Sayısal Verileri Yardımıyla araştırılması. *I. Ulusal Kar Kongresi*, Köy Hiz. (1998). Gen. Müd. Erzurum Araştırma Enstitüsü Yayınları, 70. [05.09.2008] (press Turkish).
10. Thompson, L. G. et al. Kilimanjaro ice core records: Evidence of holocene climate change in tropical Africa. *Science* **298**(5593), 589–593. <https://doi.org/10.1126/science.1073198> (2002).
11. Paul, F., Kääb, A., Maisch, M., Kellenberger, T. & Haeberli, W. Rapid disintegration of alpine glaciers observed with satellite data. *GRL* <https://doi.org/10.1029/2004GL020816> (2004).
12. Silverio, W. & Jaquet, J. M. Glacial cover mapping (1987–1996) of the cordillera Blanca (Peru) using satellite imagery. *RSE* **95**(3), 342–350. <https://doi.org/10.1016/j.rse.2004.12.012> (2005).
13. Çakır, G. Establishing spatial data base for forest management planning using remote sensing and geographic information systems. In *PhD Thesis*, Karadeniz Technical University, Graduate School Natural Applied Science. (2006).
14. Bolch, T. Climate change and glacier retreat in Northern Tien Shan (Kazakhstan/Kyrgyzstan) using remote sensing data. *Global Planet. Change.* **56**(1–2), 1–12. <https://doi.org/10.1016/j.gloplacha.2006.07.009> (2007).
15. Kim, D., Jung, H. S. & Kim, J. C. Comparison of snow cover fraction functions to estimate snow depth of South Korea from MODIS imagery. *Korean J. Remote Sens.* **33**(4), 401–410. <https://doi.org/10.7780/kjrs.2017.33.4.6> (2017).
16. Wang, Y. et al. Tracking snow variations in the Northern hemisphere using multi-source remote sensing data (2000–2015). *Remote Sens.* **10**(1), 136. <https://doi.org/10.7780/KJRS.2017.33.4.6> (2018).
17. Zakeri, F. & Mariethoz, G. Synthesizing long-term satellite imagery consistent with climate data: Application to daily snow cover. *RSE* **300**, 113877. <https://doi.org/10.1016/j.rse.2023.113877> (2024).
18. Painter, T. H., Roberts, D. A., Green, R. O. & Dozier, J. The effect of grain size on spectral mixture analysis of snow-covered area from AVIRIS data. *RSE* **65**(3), 320–332. [https://doi.org/10.1016/S0034-4257\(98\)00041-8](https://doi.org/10.1016/S0034-4257(98)00041-8) (1998).
19. Harrison, A. R. & Lucas, R. M. Multi-spectral classification of snow using NOAA AVHRR imagery. *IJRS* **10**(4–5), 907–916. <https://doi.org/10.1080/01431168908903930> (1989).

20. Hall, D. K., Foster, J. L., Salomonson, V. V., Klein, A. G. & Chien, J. Y. L. Development of a technique to assess snow-cover mapping errors from space. *TGRS* **39**(2), 432–438. <https://doi.org/10.1109/36.905251> (2001).
21. Park, S. H., Lee, M. J. & Jung, H. S. Spatiotemporal analysis of snow cover variations at mt. Kilimanjaro using multi-temporal Landsat images during 27 years. *JASTP* **143**, 37–46. <https://doi.org/10.1016/j.jastp.2016.03.007> (2016).
22. Heafner, H. & Leager, P. Monitoring of seasonal snow cover on glaciers. IGARSS. Remote Sensing: Moving Towards the 21th. Century. *Int. Geoscience and Remote Sensing Symposium*. ESA. Edinburg, UK. (1988).
23. Kawata, Y., Kusaka, T. & Ueno, S. Snowmelt runoff estimation using snow-cover extend data and its application to optimum control of dam water level. IGARSS. Remote Sensing: Moving Towards The 21th. Century. *Int. Geoscience and Remote Sensing Symposium*. ESA. Edinburg, UK. (1988).
24. Esemen, K., Güçin, M., Sunar, F. & Yavuz, V. Uydu görüntülerile karlı alan değişim analizi: Kaçkar örneği. 2. uzaktan algılama ve coğrafi bilgi sistemleri sempoziyumu UZAL-CBS, Kayseri. (2008).
25. Kazari, K., Shah-Hosseini, R. & Khanbani, S. Estimation of the surface area covered by snow and the resulting runoff using landsat satellite images. *Proceedings* **87**(1), 36 (2023). <https://doi.org/10.3390/IECG2022-13961>
26. Koç, T. & Kartum, Ş. Spatial distribution of snowfall days in Turkey. *IJE GEO* **5**(2), 218–230. <https://doi.org/10.30897/ijgeo> (2018).
27. Akyürek, Z. & Şorman, A. Ü. Monitoring snow-covered areas using NOAA-AVHRR data in the Eastern part of Turkey. *Hydrol. Sci. J.* **47**(2), 243–252. <https://doi.org/10.1080/0262660209492927> (2002).
28. Tekeli, A. E., Akyürek, Z., Şorman, A. A., Şensoy, A. & Şorman, A. Ü. Using MODIS snow cover maps in modeling snowmelt runoff process in the Eastern part of Turkey. *RSE* **97**, 216–230. <https://doi.org/10.1016/j.rse.2005.03.013> (2005).
29. URL-1. <http://www.trabzon.gov.tr/tarihce-coografya>, (2023). Accessed 06 June 2023.
30. Çakır, G. Analysis of basin characteristics for stream management using gis: A case study of Gümüşhane micro-watershed. *KUOFT* **23**(2), 144–155. <https://doi.org/10.17475/kastorman.1368097> (2023).
31. URL-2. <http://www.gumushane.gov.tr/tarihce>, (2023). Accessed 06 June 2023.
32. URL-3. <http://www.bayburt.gov.tr/tarihce>, (2023). Accessed 06 June 2023.
33. DOKAP. Doğu Karadeniz bölüm raporu, T.C. Kalkınma Bakanlığı doğu karadeniz projesi bölge kalkınma idaresi başkanlığı, Giresun. (press Turkish). (2023).
34. EarthExplorer (1999). –20223 <https://earthexplorer.usgs.gov/> path 173 row 32.
35. Deng, G. et al. Spatiotemporal dynamics of snowline altitude and their responses to climate change in the Tianshan mountains, central asia, during 2001–2019. *Sustainability* **13**, 3992. <https://doi.org/10.3390/su13073992> (2021).
36. Massom, R. A. *Satellite remote sensing of polar regions*. (Lewis Publications, 1991).
37. Konig, M., Winther, J. G. & Isaksson, E. Measuring snow and glacier ice properties from satellite. *Rev. Geophys.* **39**(1), 1–27. <https://doi.org/10.1029/1999RG000076> (2001).
38. Tong, R., Parajka, J., Komma, J. & Blöschl, G. Mapping snow cover from daily collection 6 MODIS products over Austria. *J. Hydrol.* <https://doi.org/10.1016/j.jhydrol.2020.125548> (2020).
39. Kayet, N., Pathak, K., Chakrabarty, A. & Sahoo, S. Urban heat Island explored by co-relationship between land surface temperature vs multiple vegetation indices. *Spat. Inf. Res.* **24**(5), 515–529. <https://doi.org/10.1007/s41324-016-0049-3> (2016).
40. Stillinger, T., Roberts, D. A., Collar, N. M. & Dozier, J. Cloud masking for Landsat 8 and MODIS Terra over snow-covered Terrain: Error analysis and spectral similarity between snow and cloud. *Water Resour. Res.* **55**(7), 6169–6184. <https://doi.org/10.1029/2019WR024932> (2019).
41. Dixit, A., Goswami, A., Jain, S. K. & Das, P. Remote sensing of snow cover dynamics and climate implications in the indus, ganga, and Brahmaputra river basins. *Clim. Dyn.* <https://doi.org/10.1007/s00382-024-07280-5> (2024).
42. Thapa, S. et al. Trend analysis of Climatic variables and their relation to snow cover and water availability in the central himalayas: A case study of Langtang basin, Nepal. *Theoret. Appl. Climatol.* **140**(3), 891–903. <https://doi.org/10.1007/s00704-020-03096-5> (2020).
43. Gurung, D. R. et al. Climate and topographic controls on snow cover dynamics in the Hindu Kush himalaya. *Int. J. Climatol.* **37**(10), 3873–3882. <https://doi.org/10.1002/joc.4961> (2017).
44. Liu, J. & Chen, R. Studying the Spatiotemporal variation of snow covered days over China based on combined use of MODIS snow-covered days and in situ observations. *Theoret. Appl. Climatol.* **106**, 355–363. <https://doi.org/10.1007/s00704-011-0441-9> (2011).
45. Lopez-Moreno, J. I. & Stahli, M. Statistical analysis of the snow cover variability in a subalpine watershed: Assessing the role of topography and forest interactions. *J. Hydrol.* **348**, 3–4. <https://doi.org/10.1016/j.jhydrol.2007.10.018> (2008).
46. Rohrer, M. B., Braun, L. N. & Lang, H. Long-term records of snow cover water equivalent in the Swiss alps: 1. Analysis. *Nord. Hydrol.* **25**(1–2), 53–64 (1994).
47. Woo, M. K. & Thorne, R. Snowmelt contribution to discharge from a large mountainous catchment in Subarctic canada. *Hydrol. process. Int. J.* **20**(10), 2129–2139. <https://doi.org/10.1002/hyp.6205> (2006).
48. Huang, X., Deng, J., Wang, W., Feng, Q. & Liang, T. Impact of climate and elevation on snow cover using integrated remote sensing snow products in Tibetan plateau. *RSE* **190**, 274–288. <https://doi.org/10.1016/j.rse.2016.12.028> (2017).
49. Butt, A. Q. et al. Gradual changes in snow peaks in upper indus basin, pakistan: A Google Earth based review. *J. Mt. Area Res.* **8**, 110–122. <https://doi.org/10.53874/jmar.v8i0.185> (2023).
50. Stillinger, T. et al. Landsat, MODIS, and VIIRS snow cover mapping algorithm performance as validated by airborne lidar datasets. *Cryosphere* **17**, 567–590. <https://doi.org/10.5194/tc-17-567-2023> (2023).
51. Bozali, N., Sıvrıkaya, F. & Çakır, G. An assessment of the water production value of the forest ecosystem in the Galyan basin (ATASU Dam). *BAROFT* **26**(1), 64–71. <https://doi.org/10.24011/baroef.1382944> (2024). (press Turkish).
52. Tont, S. A. & Köpeli Balıkları James Watson ve Küresel İstisna, TÜBITAK, (2008). <https://services.tubitak.gov.tr/edergi/edergi.htm>
53. Wang, Y., Su, J., Zhai, X., Meng, F. & Liu, C. Snow coverage mapping by learning from Sentinel-2 satellite multispectral images via machine learning algorithms. *Remote Sens.* **14**(3), 782 (2022).
54. Yu, Z., Gong, H., Zhang, S. & Wang, W. Snow cover extraction from Landsat 8 Oli based on deep learning with cross-scale edge-aware and attention mechanism. *Remote Sens.* **16**(18), 3430 (2024).
55. Çiftçi, B. B., Kuter, S., Akyürek, S. Z. & Weber, G. W. Fractional snow cover mapping by artificial neural networks and support vector machines. *ISPRS Annals Photogrammetry Remote Sens. Spat. Inform. Sci.* **IV-4/W4**, 179–184 (2017).

Acknowledgements

We would like to thank the relevant organization for providing Landsat satellite images from the website “<https://earthexplorer.usgs.gov/>“. This image sections are path 173 row 032 in website.

Author contributions

Günay ÇAKIR: Conceptualization, Methodology, Software. Nuri BOZALI, Fatih SİVRİKAYA.: Data curation, Writing- Original draft preparation. Günay ÇAKIR: Visualization, Investigation. Fatih SİVRİKAYA: Supervision. Günay ÇAKIR: Software, Validation. Günay ÇAKIR, Nuri BOZALI, Fatih SİVRİKAYA: Writing- Reviewing and Editing,

Declarations

Competing interests

The authors declare no competing interests.

Additional information

Correspondence and requests for materials should be addressed to G.C.

Reprints and permissions information is available at www.nature.com/reprints.

Publisher's note Springer Nature remains neutral with regard to jurisdictional claims in published maps and institutional affiliations.

Open Access This article is licensed under a Creative Commons Attribution-NonCommercial-NoDerivatives 4.0 International License, which permits any non-commercial use, sharing, distribution and reproduction in any medium or format, as long as you give appropriate credit to the original author(s) and the source, provide a link to the Creative Commons licence, and indicate if you modified the licensed material. You do not have permission under this licence to share adapted material derived from this article or parts of it. The images or other third party material in this article are included in the article's Creative Commons licence, unless indicated otherwise in a credit line to the material. If material is not included in the article's Creative Commons licence and your intended use is not permitted by statutory regulation or exceeds the permitted use, you will need to obtain permission directly from the copyright holder. To view a copy of this licence, visit <http://creativecommons.org/licenses/by-nc-nd/4.0/>.

© The Author(s) 2025